1521-0103/350/1/46–55$25.00
THE JOURNAL OF PHARMACOLOGY AND EXPERIMENTAL THERAPEUTICS

http://dx.doi.org/10.1124/jpet.113.212407
J Pharmacol Exp Ther 350:46–55, July 2014

Pharmacology of a Central Nervous System Delivered 2′-*O*-Methoxyethyl–Modified Survival of Motor Neuron Splicing Oligonucleotide in Mice and Nonhuman Primates[S]

Frank Rigo, Seung J. Chun, Daniel A. Norris, Gene Hung, Sam Lee, John Matson, Robert A. Fey, Hans Gaus, Yimin Hua, John S. Grundy, Adrian R. Krainer, Scott P. Henry, and C. Frank Bennett

Isis Pharmaceuticals, Carlsbad, California (F.R., S.J.C., D.A.N., G.H., S.L., J.M., R.A.F., H.G., J.S.G., S.P.H., C.F.B.); and Cold Spring Harbor Laboratory, Cold Spring Harbor, New York (Y.H., A.R.K.)

Received December 20, 2013; accepted April 28, 2014

ABSTRACT

Spinal muscular atrophy (SMA) is a debilitating neuromuscular disease caused by the loss of survival of motor neuron (SMN) protein. Previously, we demonstrated that ISIS 396443, an antisense oligonucleotide (ASO) targeted to the *SMN2* pre-mRNA, is a potent inducer of *SMN2* exon 7 inclusion and SMN protein expression, and improves function and survival of mild and severe SMA mouse models. Here, we demonstrate that ISIS 396443 is the most potent ASO in central nervous system (CNS) tissues of adult mice, compared with several other chemically modified ASOs. We evaluated methods of ISIS 396443 delivery to the CNS and characterized its pharmacokinetics and pharmacodynamics in rodents and nonhuman primates (NHPs). Intracerebroventricular bolus injection is a more efficient method of delivering ISIS 396443 to the CNS of rodents, compared with i.c.v. infusion. For both methods of delivery, the duration of ISIS 396443–mediated *SMN2* splicing correction is long lasting, with maximal effects still observed 6 months after treatment discontinuation. Administration of ISIS 396443 to the CNS of NHPs by a single intrathecal bolus injection results in widespread distribution throughout the spinal cord. Based upon these preclinical studies, we have advanced ISIS 396443 into clinical development.

Introduction

In its most severe form, spinal muscular atrophy (SMA) is the leading genetic cause of infant mortality (Lunn and Wang, 2008). The disease manifests as a neuromuscular disorder with severe muscle weakness and atrophy of the voluntary muscles of the limbs and trunk, with eventual paralysis as a result of the degeneration of motor neurons in the anterior horn of the spinal cord (Crawford and Pardo, 1996). The genetic basis of SMA is the loss of function of the survival of motor neuron (SMN) protein caused by deletion or, more rarely, by mutations in the *SMN1* gene (Lefebvre et al., 1995). Even though no consensus has emerged on how the reduction in levels of SMN protein causes disease, it is widely believed that a recovery in the levels of SMN protein should provide a therapeutic benefit (Burghes and Beattie, 2009).

The primary modifier of SMA is the *SMN2* gene, a paralog of *SMN1*. In humans, *SMN2* is often present in multiple copies, and patients who have a greater number of copies usually have a less severe form of the disease (Feldkotter et al., 2002; Prior et al., 2004). This is because the *SMN2* gene expresses a small amount of SMN protein due to a mutation in exon 7 that augments its alternative splicing (Coovert et al., 1997; Lefebvre et al., 1997; Lorson et al., 1999; Monani et al., 1999). Omission of exon 7 results in the production of a protein truncated at the C terminus that is unstable and rapidly degraded (Cho and Dreyfuss, 2010). Therefore, the gene-dosage effect arises because a greater number of *SMN2* copies results in a larger amount of full-length SMN protein produced (Monani et al., 2000).

Numerous approaches have been developed to increase the levels of SMN protein. These include small molecules to augment *SMN2* transcription, correct *SMN2* splicing, cause translational readthrough, and stabilize *SMN2* transcripts (Lunn and Wang, 2008); *SMN* gene delivery to replace SMN protein (Foust et al., 2010; Passini et al., 2010); antisense oligonucleotide (ASO)–based approaches to correct *SMN2* splicing (Lim and Hertel, 2001; Miyajima et al., 2002; Cartegni and Krainer, 2003; Skordis et al., 2003; Singh et al., 2006; Hua et al., 2007, 2008, 2011; Dickson et al., 2008; Williams et al., 2009; Osman et al., 2012;

Y.H. and A.R.K. were supported by the National Institutes of Health National Institute of General Medical Sciences [Grant R37-GM42699].
F.R., S.J.C., D.A.N., G.H., S.L., J.M., R.A.F., H.G., J.S.G., S.P.H., and C.F.B. are employees of Isis Pharmaceuticals. A.R.K. serves on the scientific advisory board of two nonprofit spinal muscular atrophy foundations and is a consultant for Isis Pharmaceuticals.
dx.doi.org/10.1124/jpet.113.212407.
[S] This article has supplemental material available at jpet.aspetjournals.org.

ABBREVIATIONS: Aif1, allograft inflammatory factor-1; ASO, antisense oligonucleotide; cEt, 2′,4′-constrained 2′-*O*-ethyl; CNS, central nervous system; CSF, cerebrospinal fluid; FL, full-length; HELISA, hybridization-based enzyme-linked immunosorbent assay; HPLC, high-performance liquid chromatography; HPLC-UV, high-performance liquid chromatography coupled with UV detection; ISS-N1, intronic splicing silencer N1; 2′-MOE, 2′-*O*-methoxyethyl; NBF, neutral buffered formalin; NHP, nonhuman primate; 2′-OMe, 2′-*O*-methyl; PMO, phosphorodiamidate morpholino; RT-PCR, reverse-transcription polymerase chain reaction; SMA, spinal muscular atrophy; SMN, survival of motor neuron.

Porensky et al., 2012; Mitrpant et al., 2013; Zhou et al., 2013); and antisense-producing vector-based strategies (Geib and Hertel, 2009; Meyer et al., 2009), including trans-splicing (Coady et al., 2007; Coady and Lorson, 2010). Some of these strategies have not yet been tested in animal models of SMA, but others have already been shown to be beneficial (Bebee et al., 2012).

ISIS 396443 (also known as ISIS-SMN$_{Rx}$, and previously referred to as ASO-10-27) targets a site in intron 7, termed ISS-N1, that was previously shown to repress *SMN2* exon 7 inclusion (Singh et al., 2006). Hybridization of ISIS 396443 to ISS-N1 prevents the recruitment of the splicing repressor heterogeneous nuclear ribonucleoprotein A1 and A2, and results in almost complete *SMN2* exon 7 inclusion in cell culture (Hua et al., 2008; Rigo et al., 2012). Robust splicing correction and SMN protein production are also observed in the central nervous system (CNS) of mice transgenic for *SMN2* after central administration of ISIS 396443 (Hua et al., 2010). In addition, in two severe SMA mouse models, central administration of the ASO delays the loss of motor neurons, preserves neuromuscular junctions, improves muscle physiology, and increases survival (Hua et al., 2011; Passini et al., 2011). Remarkably, peripheral administration of ISIS 396443 shows a much more profound improvement in survival, in line with mounting evidence indicating that the severe SMA mouse models have significant peripheral defects (Hamilton and Gillingwater, 2013).

Here, we have expanded the preclinical characterization of ISIS 396443. We compared ISIS 396443 to several other chemically modified ASOs to identify the most potent ASO for *SMN2* splicing correction in the CNS of adult rodents. We also assessed methods of delivering ISIS 396443 to the CNS, and characterized its pharmacokinetic and pharmacodynamic properties in rodents and nonhuman primates (NHPs).

Materials and Methods

Oligonucleotides. Synthesis and purification of all chemically modified oligonucleotides were performed as previously described (Swayze et al., 2007). For chemically modified oligonucleotides, see Supplemental Table 1, and for DNA primers, see Supplemental Table 2.

Dosing of Mice. All protocols met ethical standards for animal experimentation and were approved by the Institutional Animal Care and Use Committee. Adult male and female SMA type III mice (*Smn*$^{-/-}$; *SMN2*$^{+/+}$) were obtained from The Jackson Laboratory [FVB.Cg-Tg(SMN2)2HungSMN1tm1Hung/J, stock number 005058; Bar Harbor, ME]. The lyophilized ASOs were dissolved in sterile phosphate-buffered saline without calcium or magnesium and quantified by UV spectrometry. The ASOs were then diluted to the desired concentration required for dosing mice and sterilized through a 0.2-μm filter. Intracerebroventricular infusions (Hua and Krainer, 2012) and i.p. bolus injections (Rigo et al., 2012) were performed as previously described. For i.c.v. bolus injections, mice were placed in a stereotaxic frame and anesthetized with 2% isoflurane by a nose cone fitted into the frame. The scalp and anterior back were then shaved and disinfected. A 1–1.5-cm incision was made in the scalp, and the subcutaneous tissue and periosteum were scraped from the skull with a sterile cotton-tipped applicator. A 10-μl Hamilton microsyringe with a 26 G Huber point removable needle was used to punch through the skull at 0.2 mm posterior and 1.0 mm lateral to the bregma, and was lowered to a depth of 3 mm. Five microliters of ASO solution was injected a single time into the right lateral ventricle at a rate of 1 μl/s. After 5 minutes, the needle was slowly withdrawn and the incision was sutured. The mice were then allowed to recover from the anesthesia in their home cage.

Dosing of Nonhuman Primates. NHP studies were performed at Northern Biomedical Research, and were approved by the Institutional Animal Care and Use Committee. Male and female cynomolgus monkeys weighing 2–5 kg were anesthetized and implanted with intrathecal indwelling catheters. The monkeys were allowed to recover from the implantation surgery for several days. Solutions (100 mg/ml) of ASO were diluted to the desired final concentration in artificial cerebrospinal fluid (CSF). Monkeys received ASO in a single 1-ml i.t. bolus injection that lasted 3 minutes. Tissues were collected for analysis 7 days after the injection.

Reverse-Transcription Polymerase Chain Reaction. For spinal cord, a 2-mm lumbar section was collected. For brain, a 1-mm coronal section, 2 mm posterior to the injection site, was collected. For liver, a 3-mm^3 punch was collected. Each piece of tissue was homogenized in a 2-ml tube containing Lysing Matrix D (MP Biomedicals, Santa Ana, CA), 500 μl of RLT buffer (Qiagen, Valencia, CA), and 1% (v/v) β-mercaptoethanol. Homogenization was performed for 20 seconds at 6000 rpm using a FastPrep Automated Homogenizer (MP Biomedicals). Ten microliters of lysate was used to isolate RNA with an RNeasy 96 Kit (Qiagen) that included in-column DNA digestion with 50 U of DNase I (Invitrogen, Carlsbad, CA). Real-time reverse-transcription polymerase chain reaction (RT-PCR) was performed as previously described (Rigo et al., 2012). For Supplemental Fig. 11, RNA was isolated with an RNeasy 96 Kit (Qiagen) that included in-column DNA digestion with 30 U of DNase I (Invitrogen). Real-time RT-PCR was performed as previously described (Rigo et al., 2012). The FL or Δ7 *SMN2* expression level was normalized to either that of *Gapdh* or total *SMN2*, and this was further normalized to the level in phosphate-buffered saline–treated mice or untreated cells. For the analysis of allograft inflammatory factor-1 (*Aif1*) expression, normalization was to the levels of *Gapdh*. For Supplemental Figs. 9A and 17, RNA was isolated with an RNeasy Mini Kit (Qiagen). In-column DNA digestion was done with 50 U of DNase I (Invitrogen). For Supplemental Fig. 9A, radioactive RT-PCR was performed as previously described (Hua and Krainer, 2012). For Supplemental Fig. 17, 500 ng of RNA was reverse transcribed using oligo(dT) as the primer and SuperScript II reverse transcriptase (Invitrogen). PCR was performed with Platinum Taq DNA polymerase (Invitrogen). Amplification was conducted for 30 cycles (94°C for 30 seconds, 55°C for 30 seconds, and 72°C for 36 seconds). All PCR products were separated by agarose gel electrophoresis and stained with ethidium bromide.

Quantification of ASO Tissue Concentration. For rodents, a 1-mm brain coronal section, 3 mm posterior to the injection site and the thoracic spinal cord, was collected for bioanalytical evaluation. A 2-mm coronal brain section immediately posterior to the injection site and a 2-mm cervical spinal cord section were preserved in 10% neutral buffered formalin (NBF) for immunostaining as described later. For NHPs, the brain was sectioned in a brain matrix at 3-mm coronal slice thickness. The first slice and every other slice were frozen for bioanalytical evaluation. The interleaved brain slices were preserved in 10% NBF for immunostaining. The spinal cord was divided into lumbar, thoracic, and cervical sections, and a 1-cm portion of the rostral end of each was frozen for bioanalytical analysis. The remaining portion of each section was fixed in 10% NBF for immunostaining. Each piece of tissue was weighed, and the amount of ASO was then measured by various bioanalytical methods (Yu et al., 2013), including capillary gel electrophoresis coupled with UV detection, high-performance liquid chromatography (HPLC) coupled with UV detection (HPLC-UV), HPLC coupled with tandem mass spectrometry detection, or a hybridization-based enzyme-linked immunosorbent assay (HELISA). For HELISA, the probe has a sequence complementary to ISIS 396443 and contains biotin-triethylene glycol (TEG) at the 5′ end and digoxigenin at the 3′ end.

Immunostaining. Staining of the ASO and SMN protein in mouse tissues was performed as previously described (Hua et al., 2010). Staining of ASO in NHP tissues was performed as previously described (Kordasiewicz et al., 2012).

Plasma Chemistry. Plasma alanine aminotransferase, aspartate aminotransferase, and blood urea nitrogen concentrations were quantified on an Olympus AU400e automated clinical chemistry analyzer (Olympus, Melville, NY).

Data Analysis. The ED$_{50}$ was calculated using GraphPad Prism version 6.0 or higher (GraphPad Software, San Diego, CA) after fitting

the data using nonlinear regression with normalized response and variable slope. The ED_{50} was not calculated for experiments with a 3-point dose response. The EC_{50} and IC_{50} (half-maximal inhibitory concentration) were determined after fitting the data points to a sigmoidal E_{max} model or sigmoidal I_{max} model, respectively, using Phoenix WinNonlin 6.0 or higher (Pharsight Corporation, Mountain View, CA). For EC_{50} and IC_{50} determinations, E_0 values were fixed to be near 1.0 (0.8–1.2) to improve the curve fit. In addition, EC_{50} and IC_{50} values were bounded to be within reasonable physiologic limits. The tissue half-life of ISIS 396443 associated with the apparent terminal elimination phase was calculated using a noncompartmental analysis extravascular input model applied to the mean concentration-time profile using Phoenix WinNonlin, Version 6.0 or higher.

Results

Intracerebroventricular Infusion versus Intracerebroventricular Bolus Injection of ISIS 396443 in Rodents. Previously, we demonstrated that administration of ISIS 396443 by i.c.v. infusion into the CSF of adult mice transgenic for human *SMN2* results in almost complete *SMN2* exon 7 inclusion in CNS tissues (Fig. 1A; Supplemental Fig. 1A) (Hua et al., 2010). However, for phenotypic rescue experiments in mouse models of severe SMA, which required treating neonatal mice, we administered ISIS 396443 by i.c.v. bolus injection (Hua et al., 2011; Passini et al., 2011). Here, we directly compared the two methods of administration in adult homozygous SMA mice ($Smn^{-/-}$; $SMN2^{+/+}$) (Hsieh-Li et al., 2000) with four copies of an *SMN2* transgene to determine which method of delivery was most efficient. Increasing doses of ISIS 396443 were infused into the CSF for 7 days (Fig. 1A) or administered as a single i.c.v. bolus injection (Fig. 1D). Tissues were analyzed for *SMN2* splicing 2 days after the end of the infusion or 9 days after a single bolus injection, using real-time RT-PCR. For both methods of delivery, administration of ISIS 396443 resulted in a dose-dependent increase in *SMN2* splicing correction, observed as an increase in transcripts including exon 7 (FL) and a decrease in transcripts excluding exon 7 (Δ7), in both the spinal cord (Fig. 1, A and D) and the brain (Supplemental Fig. 1, A and D). We also examined *SMN2* splicing 71 days after the end of the 30-μg/day i.c.v. infusion and found that the level of correction in the spinal cord and brain (data not shown) was comparable to the level observed 2 days after the end of the infusion (Fig. 1A; Supplemental Fig. 1A). However, the i.c.v. bolus injection was a more efficient method of delivery, based on the half-maximal effective dose (ED_{50}). The ED_{50} for *SMN2* exon 7 inclusion following i.c.v. bolus injection was calculated to be 17 μg for the spinal cord (Fig. 1D) and 35 μg for the brain (Supplemental Fig. 1D) compared to 105 μg (15 μg/day) for the spinal cord (Fig. 1A) and 147 μg (21 μg/day) for the brain (Supplemental Fig. 1A) when ISIS 396443 was administered by i.c.v. infusion.

We also examined the relationship between the amount of ISIS 396443 in CNS tissue and the degree of *SMN2* splicing correction after both i.c.v. infusion and i.c.v. bolus injection. For each mouse that was dosed in Fig. 1, A and D, we measured the amount of ISIS 396443 in CNS tissue using HPLC-UV or HELISA, and this was plotted against the level of transcripts including exon 7 or the level of transcripts excluding exon 7 in the spinal cord and brain of the same mouse. For both routes of administration, we observed a good correlation between the amount of ISIS 396443 in CNS tissue and the levels *SMN2* splicing correction for the spinal cord (Fig. 1, B and E) and brain (Supplemental Fig. 1, B and E). However, the i.c.v. bolus injection of ISIS 396443 was a more efficient method of delivery, based on the EC_{50}. The EC_{50} was calculated to be 1.6 μg of ISIS 396443 per gram of spinal cord tissue (1.6 μg/g) (Fig. 1E) and 5.7 μg/g for the brain (Supplemental Fig. 1E) compared with 9.3 μg/g for the spinal cord (Fig. 1B) and 20.2 μg/g for the brain (Supplemental Fig. 1B) when ISIS 396443 was administered by i.c.v. infusion. Similar EC_{50} values for the spinal cord (1.2 μg/g) and brain (3.7 μg/g) were obtained when ISIS 396443 was injected by i.c.v. bolus to the C/C mouse model (Osborne et al., 2012) (Supplemental Fig. 3, B and E). Interestingly, when ISIS 396443 was administered by i.p. bolus injection, the EC_{50} value (135 μg/g) obtained in the liver was considerably higher (Supplemental Fig. 4B).

We evaluated the CNS tissue distribution of ISIS 396443 after i.c.v. bolus injection. The localization of ISIS 396443 was determined by immunohistochemistry 9 days after a 350-μg injection. ISIS 396443 distributed broadly throughout the spinal cord and brain, with accumulation in cortical, striatal, hippocampal, and motor neurons (Supplemental Fig. 2A). Consistent with the accumulation of ISIS 396443 in CNS tissues (Supplemental Fig. 2A) and efficient correction of *SMN2* splicing (Fig. 1D; Supplemental Fig. 1D), we also observed elevated levels of SMN protein in the spinal cord and brain, as determined by immunohistochemistry (Supplemental Fig. 2B).

We also determined if administration of ISIS 396443 by either i.c.v. infusion or i.c.v. bolus injection (Fig. 1) resulted in the induction of *Aif1*, a marker of monocyte/microglial activation. We examined the expression of *Aif1* in CNS tissues using real-time RT-PCR. Regardless of the method of administration, we observed no marked increase of *Aif1* transcripts in the spinal cord (Fig. 1, C and F) and brain (Supplemental Fig. 1, C and F) (Hua et al., 2010) at any dose of ISIS 396443 tested.

ISIS 396443 Duration of Action after Intracerebroventricular Infusion or Intracerebroventricular Bolus Injection in Rodents. Previously, we demonstrated that a 7-day i.c.v. infusion of ISIS 396443 at 50 μg/day resulted in sustained *SMN2* splicing correction for up to 6 months (Hua et al., 2010). To determine if *SMN2* splicing correction could be maintained for a longer period of time, adult *SMN2* transgenic mice were treated by i.c.v. infusion with 50 μg/day for 7 days (350 μg total), and *SMN2* splicing was measured by real-time RT-PCR in the spinal cord and brain at various time points. Following i.c.v. infusion of ISIS 396443, *SMN2* splicing correction in the spinal cord (Fig. 2A) and brain (Supplemental Fig. 5A) was maintained for at least 1 year, with no signs of microglial activation (Fig. 2B; Supplemental Fig. 5B). A single i.c.v. bolus injection of 100 μg of ISIS 396443 also resulted in prolonged pharmacological activity that was maintained for at least 36 weeks postdosing in the spinal cord (Fig. 2D) and brain (Supplemental Fig. 5C) without causing microglial activation (Fig. 2E; Supplemental Fig. 5D). Similar results were obtained with an i.c.v. bolus injection of 25 μg (Supplemental Fig. 6, A–D). In contrast, the duration of action of ISIS 396443 in the liver after i.p. bolus injection was much shorter, with minimal *SMN2* splicing correction observed 8 weeks after dosing (Supplemental Fig. 9A).

Since the pharmacological effects of ISIS 396443 lasted many months, we wondered if the levels of ISIS 396443 in CNS tissues changed over time. We measured the ASO levels in the spinal cord and brain by HPLC-UV or HELISA at various time points after the i.c.v. infusion or i.c.v. bolus injection and

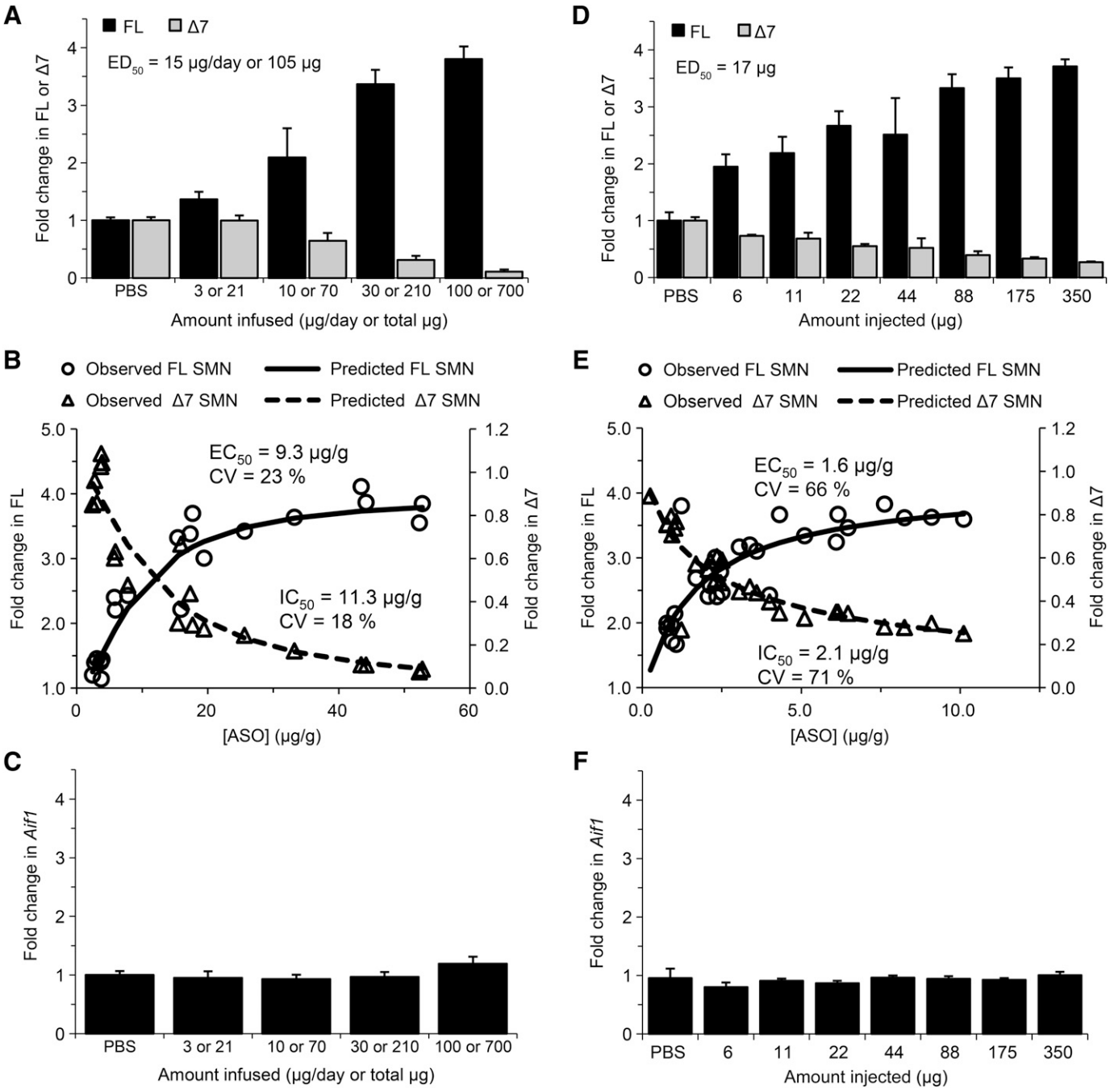

Fig. 1. Administration of ISIS 396443 by i.c.v. infusion or i.c.v. bolus injection. (A) Real-time RT-PCR analysis of *SMN2* transcripts including exon 7 (FL) or excluding exon 7 (Δ7) in the lumbar spinal cord 2 days after administration of ISIS 396443 by i.c.v. infusion for 7 days at the indicated daily doses. For each dose level, $n = 5$. Error bars represent the S.D. The calculated ED_{50} is shown. (B) For each mouse dosed in (A), the amount of ISIS 396443 in the thoracic spinal cord was measured by HPLC-UV, and this was plotted against the level of FL or Δ7 *SMN2* transcripts measured in the lumbar spinal cord of the same mouse (open circles and triangles, respectively). The calculated EC_{50} and IC_{50} values are shown. (C) Same as in A, except the real-time RT-PCR analysis was for *Aif1* transcripts. (D) Real-time RT-PCR analysis of FL and Δ7 *SMN2* transcripts in the lumbar spinal cord 9 days after administration of ISIS 396443 by a single i.c.v. bolus injection at the indicated dose. For each dose level, $n = 4$. Error bars represent the S.D. The calculated ED_{50} is shown. (E) Same as in B, except the amount of ISIS 396443 in the thoracic spinal cord was measured by HELISA. (F) Same as in D, except the real-time RT-PCR analysis was for *Aif1* transcripts. A and C are reproduced with permission from Hua et al. (2010) (Copyright 2010, Cold Spring Harbor Laboratory Press). CV, coefficient of variation; PBS, phosphate-buffered saline.

calculated the tissue half-life. Both the i.c.v. infusion and i.c.v. bolus injection of ISIS 396443 yielded a tissue half-life of over 100 days in the spinal cord and the brain (Fig. 2, C and F; Supplemental Fig. 6E). Therefore, the long-lasting pharmacodynamic effects of ISIS 396443 can be attributed to its long tissue half-life. For many months after dosing, ISIS 396443 remains at sufficient levels in CNS tissues to modulate splicing. Mass spectrometry analysis of CNS tissues indicated minimal metabolism of ISIS 396443, with the main metabolite being the parent compound that lacked a 3′-terminal guanosine (data not shown). In agreement with the long pharmacological effects and tissue half-life, ISIS 396443 could be detected in motor neurons

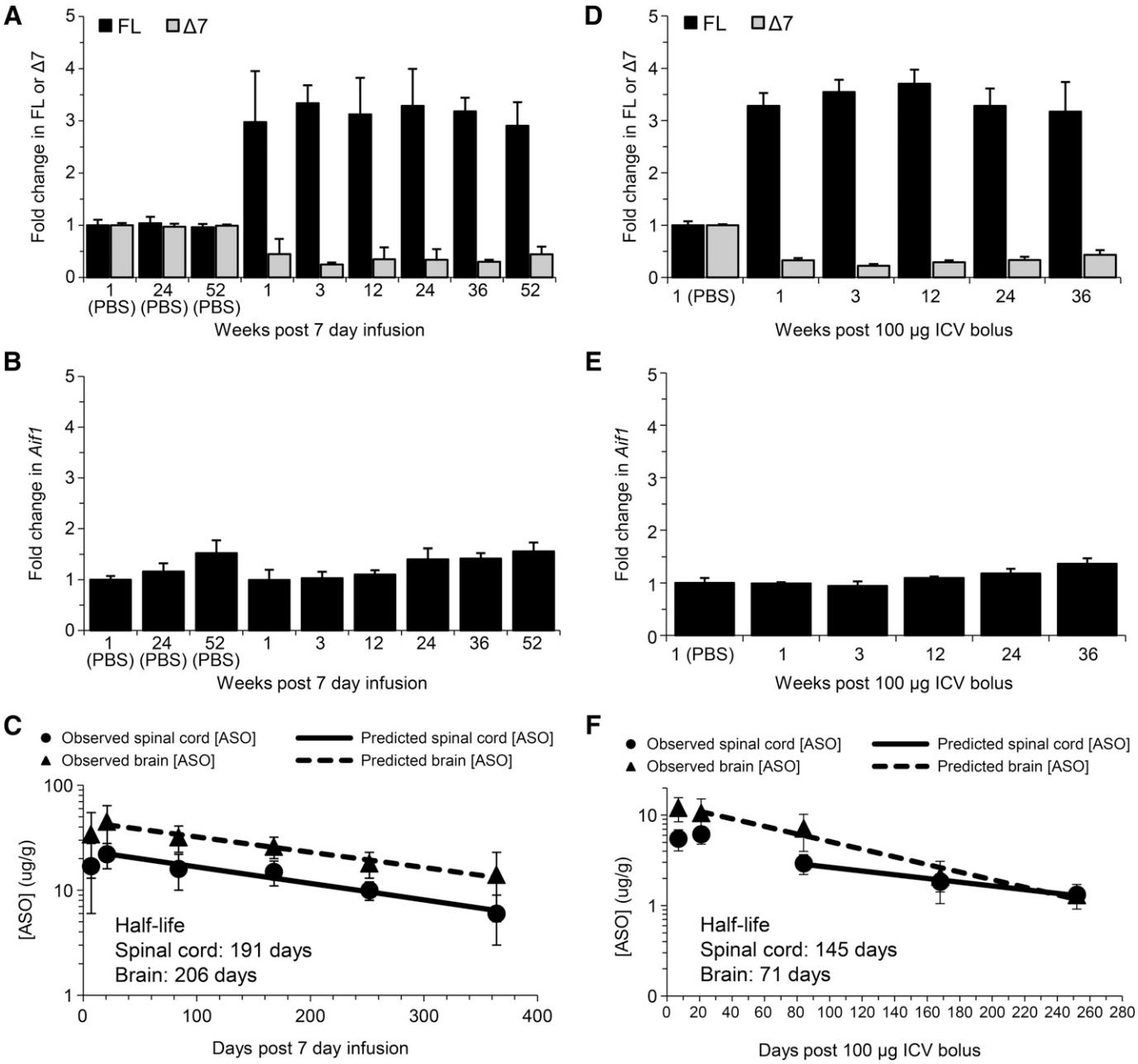

Fig. 2. Duration of action after i.c.v. infusion or i.c.v. bolus injection of ISIS 396443. (A) Real-time RT-PCR analysis of *SMN2* FL and Δ7 transcripts in the lumbar spinal cord at the indicated time points after administration of ISIS 396443 by i.c.v. infusion at 50 μg/day for 7 days. Phosphate-buffered saline (PBS), n = 4; 1 and 3 weeks, n = 5; 12 weeks, n = 6; 24 weeks, n = 7; 36 weeks, n = 6; 52 weeks n = 7. Error bars represent the S.D. (B) Same as in A, except that the real-time RT-PCR analysis was for *Aif1* transcripts. (C) The amount of ISIS 396443 in the thoracic spinal cord or brain of each mouse was measured at each time point by HPLC-UV. One and 3 weeks, n = 5; 12 weeks, n = 6; 24 weeks, n = 7; 36 weeks, n = 6; 52 weeks, n = 7. Error bars represent the S.D. The calculated tissue half-life of ISIS 396443 is shown. (D) Real-time RT-PCR analysis of FL and Δ7 *SMN2* transcripts in the lumbar spinal cord at the indicated time points after administration of 100 μg of ISIS 396443 by a single i.c.v. bolus injection. For each time point, n = 5, except for the 24-week group, for which n = 4. Error bars represent the S.D. (E) Same as in D, except the real-time RT-PCR analysis was for *Aif1* transcripts. (F) Same as in C, except the amount of ISIS 396443 in the thoracic spinal cord and brain was measured by HELISA. For each time point, n = 5, except for the 24-week group, for which n = 4. Error bars represent the S.D.

1 year after the 7-day i.c.v. infusion and 36 weeks after the i.c.v. bolus injection (Supplemental Figs. 7A and 8A). In addition, SMN protein was also present in motor neurons at these time points (Supplemental Figs. 7B and 8B). In contrast to what was observed in the CNS, the liver half-life of ISIS 396443 was about 20 days (Supplemental Fig. 9B), in agreement with the shorter duration of *SMN2* splicing correction in liver.

The long-lasting pharmacodynamic effects of ISIS 396443 in the CNS of mice are in agreement with its long tissue half-life. However, to confirm that the *SMN2* splicing correction was still driven by the presence of ISIS 396443 after its delivery, we administered a fully complementary oligonucleotide decoy (α443) to neutralize its effects. Three weeks after a 100-μg i.c.v. bolus injection of ISIS 396443, efficient *SMN2* splicing correction was observed in the spinal cord and brain (Supplemental Fig. 10, A and C). At this time point, we administered 400 μg of the complementary oligonucleotide decoy, α443, by i.c.v. bolus injection and assessed the effects on *SMN2* splicing

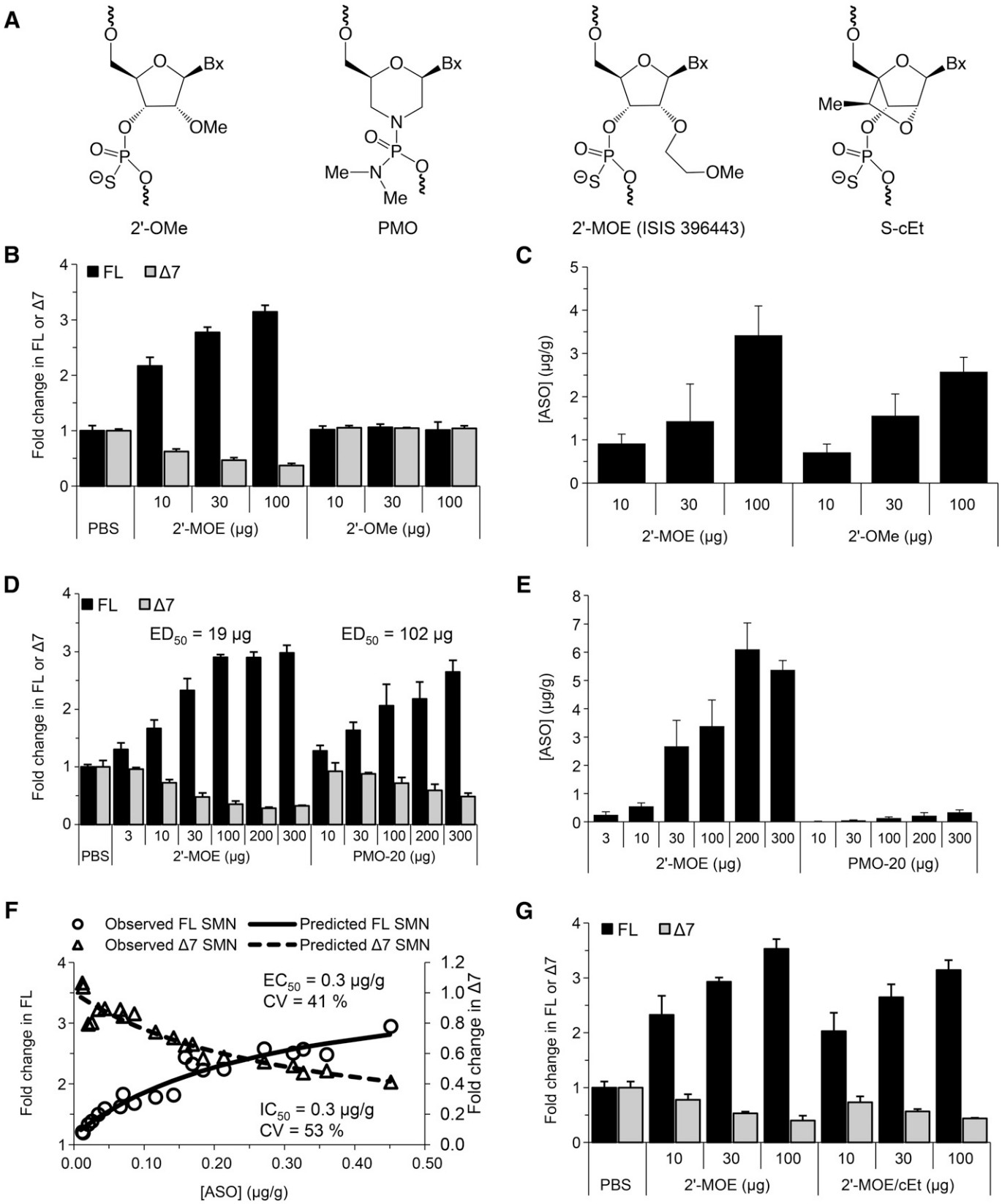

Fig. 3. Comparison of ISIS 396443 to 2′-MOE, PMO-20, and cEt ASOs. (A) Structures of chemically modified nucleotides. (B) Real-time RT-PCR analysis of FL and Δ7 *SMN2* transcripts in the lumbar spinal cord 9 days after administration of ISIS 396443 or the 2′-OMe ASO by a single i.c.v. bolus injection at the indicated dose. For each dose level, $n = 4$. Error bars represent the S.D. (C) The amount of ISIS 396443 and 2′-OMe ASO in the thoracic spinal cord of each mouse was measured by HELISA. For each dose level, $n = 4$. Error bars represent the S.D. (D) Same as B, except ISIS 396443 and the PMO-20 ASO were administered at the indicated doses. The calculated ED_{50} is shown. (E) Same as in C, except ISIS 396443 and the PMO-20 ASO were measured. (F) The concentration of the PMO-20 ASO in the thoracic spinal cord of each mouse in E was plotted against the level of FL or Δ7 *SMN2*

2 weeks later. Administration of α443 reversed the ISIS 396443–mediated splicing correction in the spinal cord and brain (Supplemental Fig. 10, A and C). Similar results were obtained when lower doses of ISIS 396443 and α443 were used (Supplemental Fig. 10, B and D).

ISIS 396443 versus 2′-*O*-Methyl, Morpholino, and 2′,4′-Constrained 2′-*O*-Ethyl ASOs in the CNS of Rodents. ASOs with 2′-*O*-methoxyethyl (2′-MOE) (Hua et al., 2011; Passini et al., 2011), 2′-*O*-methyl (2′-OMe) (Williams et al., 2009), and phosphorodiamidate morpholino (PMO) chemistries (Porensky et al., 2012; Mitrpant et al., 2013; Zhou et al., 2013) (Fig. 3A), which drive *SMN2* exon 7 inclusion, have been tested in mice with severe SMA by central administration within the first postnatal day. In these experiments, early administration of the ASOs was necessary since severe SMA mice normally die within the first weeks of life. To more adequately compare the potency of ASOs with different chemistries, to select the best ASO to advance into clinical trials, we administered them centrally to adult mice. We tested ISIS 396443, an 18-mer ASO with the 2′-MOE chemistry (Hua et al., 2008, 2010, 2011; Passini et al., 2011), and two 20-mer ASOs of the same sequence: a 2′-OMe ASO (Singh et al., 2006; Williams et al., 2009) and a PMO ASO (Porensky et al., 2012; Mitrpant et al., 2013) that were previously optimized for *SMN2* exon 7 inclusion and, similar to ISIS 396443, also target ISS-N1. Increasing doses of these ASOs were administered by a single i.c.v. bolus injection to adult *SMN2* transgenic mice, and *SMN2* splicing correction was measured by real-time RT-PCR 9 days later in CNS tissues. Consistent with our previous report (Hua et al., 2010), administration of the 2′-OMe ASO did not result in *SMN2* splicing correction in the spinal cord (Fig. 3B) and brain (Supplemental Fig. 12A) but did elevate *Aif1* expression in the spinal cord (Supplemental Fig. 12D). In this experiment, the 2′-OMe ASO did accumulate in spinal cord and brain tissue, in a dose-dependent manner, to a similar level as ISIS 396443 (Fig. 3C; Supplemental Fig. 12B). In addition, this 2′-OMe ASO was able to correct *SMN2* splicing when administered to SMA fibroblasts by lipid transfection (Supplemental Fig. 11A), but surprisingly, it was almost completely inactive when administered by electroporation (Supplemental Fig. 11C).

Administration of the PMO-20 ASO resulted in a dose-dependent increase in *SMN2* splicing correction in the spinal cord (Fig. 3D) and brain (Supplemental Fig. 14A). However, the PMO-20 ASO was not as potent as ISIS 396443 when administered to adult *SMN2* transgenic mice. For the PMO-20 ASO, the ED_{50} for *SMN2* exon 7 inclusion was calculated to be 102 μg for the spinal cord and 65 μg for the brain. This represents a 3- to 5-fold decrease in potency, as the ED_{50} for ISIS 396443 in the same experiment was calculated to be 19 μg for the spinal cord and 18 μg for the brain (Fig. 3D; Supplemental Fig. 14A). The same conclusion was reached when we tested another PMO ASO that was slightly longer (PMO-23) (Supplemental Fig. 15). In contrast, when the ASOs were administered to SMA patient fibroblasts, the PMO-20 ASO was as potent as ISIS 396443 for *SMN2* splicing correction (Supplemental Fig. 11B).

To determine if the reduced potency of the PMO-20 ASO for *SMN2* splicing correction in transgenic mice was due to its accumulation in the CNS, we measured its levels in the spinal cord and brain by HELISA. The accumulation of the PMO-20 ASO in CNS tissues was substantially lower, compared with ISIS 396443 in the spinal cord (Fig. 3E) and brain (Supplemental Fig. 14B). When we plotted the concentration of the PMO-20 ASO in the spinal cord and brain as a function of the level of *SMN2* splicing correction, we found that its EC_{50} was lower compared with ISIS 396443: 0.3 versus 1.4 μg/g in the spinal cord (Fig. 3F; Supplemental Fig. 13) and 0.8 versus 6.3 μg/g in the brain (Supplemental Fig. 14, C and D). These findings suggest that the PMO-20 ASO has less efficient tissue retention or cellular uptake than ISIS 396443. However, the smaller amount of PMO-20 ASO that is retained in tissue or taken up by cells can efficiently correct *SMN2* splicing.

The binding affinity of an ASO to its target can be increased dramatically by the incorporation of 2′,4′-bridged nucleic acid modifications, such as locked nucleic acid (Vester and Wengel, 2004) and 2′,4′-constrained 2′-*O*-ethyl (cEt) (Seth et al., 2010) (Fig. 3A). We determined if a cEt-modified version of ISIS 396443 was more active than ISIS 396443. We tested a cEt mixmer (2′-MOE/cEt) ASO, with a melting temperature 15°C higher than ISIS 396443, in SMA fibroblasts and found that its potency was similar to ISIS 396443 (Supplemental Fig. 11C). This was also the case when we administered the 2′-MOE/cEt ASO by i.c.v. bolus injection to adult *SMN2* transgenic mice (Fig. 3G; Supplemental Fig. 16). Therefore, further increasing the affinity of ISIS 396443 for binding to ISS-N1 does not increase its potency for *SMN2* splicing correction.

Pharmacokinetics of ISIS 396443 in the CNS of Nonhuman Primates. NHPs do not have the *SMN2* gene (Rochette et al., 2001) and rely on the *SMN1* gene for SMN protein production. In humans, about 10% of the transcripts produced from the *SMN1* gene exclude exon 7 (Lorson et al., 1999). We reasoned that if exon 7–skipped transcripts from the NHP *SMN1* gene could be detected in the spinal cord, we could potentially evaluate ASO-mediated *SMN1* splicing correction in a large animal. Unfortunately, we could not detect *SMN1* exon 7–skipped transcripts in the spinal cord (Supplemental Fig. 17), precluding our ability to measure pharmacodynamic effects of ISIS 396443 in NHPs. Instead, we determined whether administration of ISIS 396443 to NHPs by i.t. bolus injection resulted in a spinal cord ASO concentration that was predicted to achieve the EC_{50} (~1 μg/g) for *SMN2* splicing correction in the spinal cord of *SMN2* transgenic mice after delivery of ISIS 396443 by i.c.v. bolus. Intrathecal bolus injection is technically challenging in mice, but is feasible in NHPs. Adult cynomolgus monkeys were treated by a single i.t. bolus injection with either 1, 3, or 7 mg of ISIS 396443, and tissues were collected 7 days after dosing for processing. The accumulation of ISIS 396443 in CNS tissues was dose-dependent, with greater accumulation in the spinal cord and cortex (Fig. 4A). Even at the 1-mg dose, the levels of ISIS 396443 in the spinal cord exceeded the targeted tissue concentration of about 1 μg/g by 3- to 8-fold. Immunohistochemical staining of various regions of the spinal cord and brain for the presence of ISIS 396443 showed broad distribution of ISIS 396443, with the greatest accumulation in large and small cell bodies of the gray matter, consistent with

transcripts measured in the lumbar spinal cord of the same mouse (open circles and triangles, respectively). The calculated EC_{50} and IC_{50} values are shown. (G) Same as in B, except ISIS 396443 and the 2′-MOE/cEt ASO were administered at the indicated doses. CV, coefficient of variation.

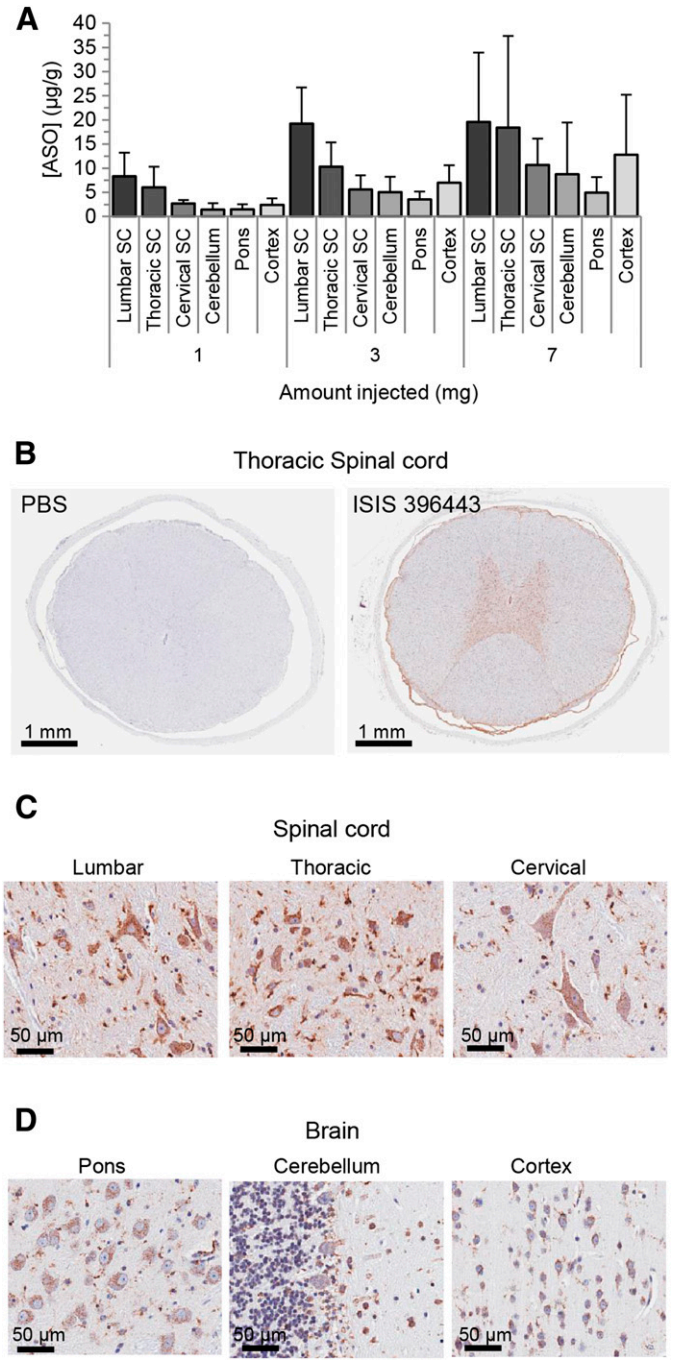

Fig. 4. Pharmacokinetics of ISIS 396443 in the CNS of nonhuman primates after a single i.t. bolus injection. (A) The amount of ISIS 396443 in various spinal cord and brain regions of each NHP was measured by HELISA. For each dose level, $n = 6$. Error bars represent the S.D. (B–D) ISIS 396443 in the CNS of a primate that received a dose of 7 mg was visualized by ASO immunostaining (antipan ASO). Nuclei were counterstained with hematoxylin. SC, spinal cord; PBS, phosphate-buffered saline.

neuronal and glial cell targeting (Fig. 4, B–D). H&E staining did not reveal any pathologic findings at the doses of ISIS 396443 tested (data not shown).

Discussion

Here, we determined that, on a per-dose basis, ISIS 396443 is the most potent ASO for *SMN2* splicing correction in the CNS of adult mice out of several ASOs tested, including an ASO with high-binding affinity chemical modifications. The most efficient method of delivering ISIS 396443 to the CNS of rodents is through an i.c.v. bolus injection, with pharmacology in CNS tissues that is long-lasting. In addition, administration of ISIS 396443 to the CNS of NHPs by a single i.t. bolus injection results in widespread distribution throughout the spinal cord and accumulation to levels predicted to be pharmacologically active, as determined from our experiments in rodents. Based upon our complete set of preclinical studies, we have advanced ISIS 396443 into clinical development.

There are several reasons why i.t. bolus injection of ISIS 396443, rather than an infusion, is being pursued in the clinic, based in part on the present study: 1) bolus injection results in potent and efficient *SMN2* splicing correction in the CNS of rodents; 2) bolus injection results in sustained *SMN2* splicing correction in the CNS of rodents for many months, which can be extrapolated to infrequent dosing in the clinic; and 3) bolus injection results in distribution of the ASO throughout the spinal cord of NHPs and accumulation in tissue at levels predicted to be pharmacologically active. In addition, for i.t. delivery of ISIS 396443 to SMA patients, the implantation of an infusion device (i.e., an implanted pump) is not feasible in small children or infants, whereas standard lumbar puncture bolus injections have been proven to be feasible and well tolerated in children (i.e., for the delivery of anesthetics and chemotherapeutics). In fact, administration of a single dose of ISIS 396443 by lumbar puncture bolus injection in children 2–14 years of age with SMA has recently been shown to be feasible and well tolerated in a completed phase 1 clinical study (Chirboga et al., 2013).

Previous studies indicate that ASOs accumulate in cells and tissues by at least two distinct uptake pathways (Bennett and Swayze, 2010). One pathway is termed the productive uptake pathway, which ultimately results in the productive engagement of the ASO with the desired target. The second pathway is a nonproductive pathway that acts as a saturable sink and impairs the ability of the ASO to reach the productive pathway. It is likely that many different nonproductive sinks exist, but some have been described as intracellular lysosomes, cell-surface proteins, or even other cell types (Geary et al., 2009; Koller et al., 2011; Ming et al., 2013). Several of our results may be explained by preferential utilization of the productive versus nonproductive ASO uptake pathway. The EC_{50} for *SMN2* splicing correction is an indicator of the amount of drug taken up into tissues via productive uptake. The lower EC_{50} in CNS tissues compared with the liver when ISIS 396443 was administered centrally versus peripherally, respectively, suggests that ISIS 396443 favors a productive uptake pathway in the CNS, compared with the liver. The lower EC_{50} in CNS tissues when ISIS 396443 was administered by i.c.v. bolus injection, which results in a higher maximum concentration in CSF, versus i.c.v. infusion, suggests that delivery of ISIS 396443 by i.c.v. bolus injection results in greater productive uptake. Perhaps the scenario in the CNS is similar to what has been observed for the liver, where administration by slow infusion results in the preferential accumulation of ASO in a nonproductive compartment (Geary et al., 2009). The lower EC_{50} for the PMO ASO versus ISIS 396443 in CNS tissues implies that a greater fraction of the PMO ASO in the tissue is found in a productive compartment, despite its diminished overall tissue accumulation, compared with ISIS 396443. Taken

together, our results demonstrate that the preferential utilization of the productive uptake pathway depends on the target tissue, the method of delivery, and the chemistry of the ASO.

The prolonged duration of *SMN2* splicing correction after a single i.c.v. bolus injection is in agreement with the slow clearance of ISIS 396443 from CNS tissues, which remains at sufficient levels to maximally correct *SMN2* splicing for many months. Because ISIS 396443 is fully modified with 2′-MOE nucleotides that confer increased nuclease resistance (Teplova et al., 1999), we expected the long tissue half-lives. However, low ASO metabolic activity in CNS tissues might also be a contributing factor (Whitesell et al., 1993). It is also interesting to consider that the long duration of antisense effects in the CNS might be attributable to the target cells being postmitotic, as long-lasting pharmacology has also been observed in muscle (Wheeler et al., 2012).

In light of the finding that ISIS 396443 is more potent for *SMN2* splicing correction in CNS tissues of adult transgenic mice compared with PMO ASOs, the longer survival conferred by i.c.v.-injected PMO ASOs (Porensky et al., 2012; Mitrpant et al., 2013; Zhou et al., 2013) compared with ISIS 396443 (Hua et al., 2011; Passini et al., 2011) in severe SMA mice is intriguing. Several possibilities may account for this paradox, including the higher doses of PMO ASOs used in neonatal mice, the longer duration of PMO ASO–mediated *SMN2* splicing correction in a growing neonatal mouse, the higher exposure of peripheral tissues to PMO ASOs after CNS administration, or enhanced activity of the PMO ASOs in certain CNS cell types. Additional studies are necessary to address the apparent paradox.

Acknowledgments

The authors thank the Isis ASO synthesis group and Thazha Prakash for ASO synthesis, and the SMA Foundation for providing the C/C mice.

Authorship Contributions

Participated in research design: Rigo, Chun, Fey, Hua, Grundy, Krainer, Henry, Bennett.

Conducted experiments: Rigo, Chun, Lee.

Performed data analysis: Rigo, Chun, Norris, Hung, Matson, Gaus.

Wrote or contributed to the writing of the manuscript: Rigo, Krainer, Bennett.

References

Bebee TW, Dominguez CE, and Chandler DS (2012) Mouse models of SMA: tools for disease characterization and therapeutic development. *Hum Genet* **131**:1277–1293.

Bennett CF and Swayze EE (2010) RNA targeting therapeutics: molecular mechanisms of antisense oligonucleotides as a therapeutic platform. *Annu Rev Pharmacol Toxicol* **50**:259–293.

Burghes AH and Beattie CE (2009) Spinal muscular atrophy: why do low levels of survival motor neuron protein make motor neurons sick? *Nat Rev Neurosci* **10**:597–609.

Cartegni L and Krainer AR (2003) Correction of disease-associated exon skipping by synthetic exon-specific activators. *Nat Struct Biol* **10**:120–125.

Chirboga C, Swoboda K, Darras B, Iannaccone S, Montes J, Allen H, Parad R, Johnson S, De Vivo D, Norris D et al.(2013) Results of an open-label, escalating dose study to assess the safety, tolerability, and dose range finding of a single intrathecal dose of ISIS-SMNRx in patients with spinal muscular atrophy, in *65th American Academy of Neurology Annual Meeting*; 16–23 March 2013; San Diego, CA.Vol 80, ppS S36.002, American Academy of Neurology, Minneapolis, MN.

Cho S and Dreyfuss G (2010) A degron created by SMN2 exon 7 skipping is a principal contributor to spinal muscular atrophy severity. *Genes Dev* **24**:438–442.

Coady TH and Lorson CL (2010) Trans-splicing-mediated improvement in a severe mouse model of spinal muscular atrophy. *J Neurosci* **30**:126–130.

Coady TH, Shababi M, Tullis GE, and Lorson CL (2007) Restoration of SMN function: delivery of a trans-splicing RNA re-directs SMN2 pre-mRNA splicing. *Mol Ther* **15**: 1471–1478.

Coovert DD, Le TT, McAndrew PE, Strasswimmer J, Crawford TO, Mendell JR, Coulson SE, Androphy EJ, Prior TW, and Burghes AH (1997) The survival motor neuron protein in spinal muscular atrophy. *Hum Mol Genet* **6**:1205–1214.

Crawford TO and Pardo CA (1996) The neurobiology of childhood spinal muscular atrophy. *Neurobiol Dis* **3**:97–110.

Dickson A, Osman E, and Lorson CL (2008) A negatively acting bifunctional RNA increases survival motor neuron both in vitro and in vivo. *Hum Gene Ther* **19**: 1307–1315.

Feldkötter M, Schwarzer V, Wirth R, Wienker TF, and Wirth B (2002) Quantitative analyses of SMN1 and SMN2 based on real-time lightCycler PCR: fast and highly reliable carrier testing and prediction of severity of spinal muscular atrophy. *Am J Hum Genet* **70**:358–368.

Foust KD, Wang X, McGovern VL, Braun L, Bevan AK, Haidet AM, Le TT, Morales PR, Rich MM, and Burghes AH, et al. (2010) Rescue of the spinal muscular atrophy phenotype in a mouse model by early postnatal delivery of SMN. *Nat Biotechnol* **28**: 271–274.

Geary RS, Wancewicz E, Matson J, Pearce M, Siwkowski A, Swayze E, and Bennett F (2009) Effect of dose and plasma concentration on liver uptake and pharmacologic activity of a 2′-methoxyethyl modified chimeric antisense oligonucleotide targeting PTEN. *Biochem Pharmacol* **78**:284–291.

Geib T and Hertel KJ (2009) Restoration of full-length SMN promoted by adenoviral vectors expressing RNA antisense oligonucleotides embedded in U7 snRNAs. *PLoS ONE* **4**:e8204.

Hamilton G and Gillingwater TH (2013) Spinal muscular atrophy: going beyond the motor neuron. *Trends Mol Med* **19**:40–50.

Hsieh-Li HM, Chang JG, Jong YJ, Wu MH, Wang NM, Tsai CH, and Li H (2000) A mouse model for spinal muscular atrophy. *Nat Genet* **24**:66–70.

Hua Y and Krainer AR (2012) Antisense-mediated exon inclusion. *Methods Mol Biol* **867**:307–323.

Hua Y, Sahashi K, Hung G, Rigo F, Passini MA, Bennett CF, and Krainer AR (2010) Antisense correction of SMN2 splicing in the CNS rescues necrosis in a type III SMA mouse model. *Genes Dev* **24**:1634–1644.

Hua Y, Sahashi K, Rigo F, Hung G, Horev G, Bennett CF, and Krainer AR (2011) Peripheral SMN restoration is essential for long-term rescue of a severe spinal muscular atrophy mouse model. *Nature* **478**:123–126.

Hua Y, Vickers TA, Baker BF, Bennett CF, and Krainer AR (2007) Enhancement of SMN2 exon 7 inclusion by antisense oligonucleotides targeting the exon. *PLoS Biol* **5**:e73.

Hua Y, Vickers TA, Okunola HL, Bennett CF, and Krainer AR (2008) Antisense masking of an hnRNP A1/A2 intronic splicing silencer corrects SMN2 splicing in transgenic mice. *Am J Hum Genet* **82**:834–848.

Koller E, Vincent TM, Chappell A, De S, Manoharan M, and Bennett CF (2011) Mechanisms of single-stranded phosphorothioate modified antisense oligonucleotide accumulation in hepatocytes. *Nucleic Acids Res* **39**:4795–4807.

Kordasiewicz HB, Stanek LM, Wancewicz EV, Mazur C, McAlonis MM, Pytel KA, Artates JW, Weiss A, Cheng SH, and Shihabuddin LS, et al. (2012) Sustained therapeutic reversal of Huntington's disease by transient repression of huntingtin synthesis. *Neuron* **74**:1031–1044.

Lefebvre S, Bürglen L, Reboullet S, Clermont O, Burlet P, Viollet L, Benichou B, Cruaud C, Millasseau P, and Zeviani M, et al. (1995) Identification and characterization of a spinal muscular atrophy-determining gene. *Cell* **80**:155–165.

Lefebvre S, Burlet P, Liu Q, Bertrandy S, Clermont O, Munnich A, Dreyfuss G, and Melki J (1997) Correlation between severity and SMN protein level in spinal muscular atrophy. *Nat Genet* **16**:265–269.

Lim SR and Hertel KJ (2001) Modulation of survival motor neuron pre-mRNA splicing by inhibition of alternative 3′ splice site pairing. *J Biol Chem* **276**: 45476–45483.

Lorson CL, Hahnen E, Androphy EJ, and Wirth B (1999) A single nucleotide in the SMN gene regulates splicing and is responsible for spinal muscular atrophy. *Proc Natl Acad Sci USA* **96**:6307–6311.

Lunn MR and Wang CH (2008) Spinal muscular atrophy. *Lancet* **371**:2120–2133.

Meyer K, Marquis J, Trüb J, Nlend Nlend R, Verp S, Ruepp MD, Imboden H, Barde I, Trono D, and Schümperli D (2009) Rescue of a severe mouse model for spinal muscular atrophy by U7 snRNA-mediated splicing modulation. *Hum Mol Genet* **18**: 546–555.

Ming X, Carver K, Fisher M, Noel R, Cintrat JC, Gillet D, Barbier J, Cao C, Bauman J, and Juliano RL (2013) The small molecule Retro-1 enhances the pharmacological actions of antisense and splice switching oligonucleotides. *Nucleic Acids Res* **41**: 3673–3687.

Mitrpant C, Porensky P, Zhou H, Price L, Muntoni F, Fletcher S, Wilton SD, and Burghes AH (2013) Improved antisense oligonucleotide design to suppress aberrant SMN2 gene transcript processing: towards a treatment for spinal muscular atrophy. *PLoS ONE* **8**:e62114.

Miyajima H, Miyaso H, Okumura M, Kurisu J, and Imaizumi K (2002) Identification of a cis-acting element for the regulation of SMN exon 7 splicing. *J Biol Chem* **277**: 23271–23277.

Monani UR, Lorson CL, Parsons DW, Prior TW, Androphy EJ, Burghes AH, and McPherson JD (1999) A single nucleotide difference that alters splicing patterns distinguishes the SMA gene SMN1 from the copy gene SMN2. *Hum Mol Genet* **8**:1177–1183.

Monani UR, Sendtner M, Coovert DD, Parsons DW, Andreassi C, Le TT, Jablonka S, Schrank B, Rossoll W, and Prior TW, et al. (2000) The human centromeric survival motor neuron gene (SMN2) rescues embryonic lethality in Smn(-/-) mice and results in a mouse with spinal muscular atrophy. *Hum Mol Genet* **9**:333–339.

Osborne M, Gomez D, Feng Z, McEwen C, Beltran J, Cirillo K, El-Khodor B, Lin MY, Li Y, and Knowlton WM, et al. (2012) Characterization of behavioral and neuromuscular junction phenotypes in a novel allelic series of SMA mouse models. *Hum Mol Genet* **21**:4431–4447.

Osman EY, Yen PF, and Lorson CL (2012) Bifunctional RNAs targeting the intronic splicing silencer N1 increase SMN levels and reduce disease severity in an animal model of spinal muscular atrophy. *Mol Ther* **20**:119–126.

Passini MA, Bu J, Richards AM, Kinnecom C, Sardi SP, Stanek LM, Hua Y, Rigo F, Matson J, and Hung G, et al. (2011) Antisense oligonucleotides delivered to the

mouse CNS ameliorate symptoms of severe spinal muscular atrophy. *Sci Transl Med* **3**:72ra18.
Passini MA, Bu J, Roskelley EM, Richards AM, Sardi SP, O'Riordan CR, Klinger KW, Shihabuddin LS, and Cheng SH (2010) CNS-targeted gene therapy improves survival and motor function in a mouse model of spinal muscular atrophy. *J Clin Invest* **120**:1253–1264.
Porensky PN, Mitrpant C, McGovern VL, Bevan AK, Foust KD, Kaspar BK, Wilton SD, and Burghes AH (2012) A single administration of morpholino antisense oligomer rescues spinal muscular atrophy in mouse. *Hum Mol Genet* **21**: 1625–1638.
Prior TW, Swoboda KJ, Scott HD, and Hejmanowski AQ (2004) Homozygous SMN1 deletions in unaffected family members and modification of the phenotype by SMN2. *Am J Med Genet A* **130A**:307–310.
Rigo F, Hua Y, Chun SJ, Prakash TP, Krainer AR, and Bennett CF (2012) Synthetic oligonucleotides recruit ILF2/3 to RNA transcripts to modulate splicing. *Nat Chem Biol* **8**:555–561.
Rochette CF, Gilbert N, and Simard LR (2001) SMN gene duplication and the emergence of the SMN2 gene occurred in distinct hominids: SMN2 is unique to Homo sapiens. *Hum Genet* **108**:255–266.
Seth PP, Vasquez G, Allerson CA, Berdeja A, Gaus H, Kinberger GA, Prakash TP, Migawa MT, Bhat B, and Swayze EE (2010) Synthesis and biophysical evaluation of 2′,4′-constrained 2′O-methoxyethyl and 2′,4′-constrained 2′O-ethyl nucleic acid analogues. *J Org Chem* **75**:1569–1581.
Singh NK, Singh NN, Androphy EJ, and Singh RN (2006) Splicing of a critical exon of human Survival Motor Neuron is regulated by a unique silencer element located in the last intron. *Mol Cell Biol* **26**:1333–1346.
Skordis LA, Dunckley MG, Yue B, Eperon IC, and Muntoni F (2003) Bifunctional antisense oligonucleotides provide a trans-acting splicing enhancer that stimulates SMN2 gene expression in patient fibroblasts. *Proc Natl Acad Sci USA* **100**: 4114–4119.
Swayze EE, Siwkowski AM, Wancewicz EV, Migawa MT, Wyrzykiewicz TK, Hung G, Monia BP, and Bennett CF (2007) Antisense oligonucleotides containing locked nucleic acid improve potency but cause significant hepatotoxicity in animals. *Nucleic Acids Res* **35**:687–700.
Teplova M, Minasov G, Tereshko V, Inamati GB, Cook PD, Manoharan M, and Egli M (1999) Crystal structure and improved antisense properties of 2′-O-(2-methoxyethyl)-RNA. *Nat Struct Biol* **6**:535–539.
Vester B and Wengel J (2004) LNA (locked nucleic acid): high-affinity targeting of complementary RNA and DNA. *Biochemistry* **43**:13233–13241.
Wheeler TM, Leger AJ, Pandey SK, MacLeod AR, Nakamori M, Cheng SH, Wentworth BM, Bennett CF, and Thornton CA (2012) Targeting nuclear RNA for in vivo correction of myotonic dystrophy. *Nature* **488**:111–115.
Whitesell L, Geselowitz D, Chavany C, Fahmy B, Walbridge S, Alger JR, and Neckers LM (1993) Stability, clearance, and disposition of intraventricularly administered oligodeoxynucleotides: implications for therapeutic application within the central nervous system. *Proc Natl Acad Sci USA* **90**:4665–4669.
Williams JH, Schray RC, Patterson CA, Ayitey SO, Tallent MK, and Lutz GJ (2009) Oligonucleotide-mediated survival of motor neuron protein expression in CNS improves phenotype in a mouse model of spinal muscular atrophy. *J Neurosci* **29**:7633–7638.
Yu RZ, Grundy JS, and Geary RS (2013) Clinical pharmacokinetics of second generation antisense oligonucleotides. *Expert Opin Drug Metab Toxicol* **9**:169–182.
Zhou H, Janghra N, Mitrpant C, Dickinson RL, Anthony K, Price L, Eperon IC, Wilton SD, Morgan J, and Muntoni F (2013) A novel morpholino oligomer targeting ISS-N1 improves rescue of severe spinal muscular atrophy transgenic mice. *Hum Gene Ther* **24**:331–342.

Address correspondence to: Frank Rigo, 2855 Gazelle Court, Carlsbad, CA 92010. E-mail: frigo@isisph.com